Advanced Steel Construction – Vol. 19 No. 3 (2023) 185–196
DOI:10.18057/IJASC.2023.19.3.1

SEISMIC BEHAVIOR OF BUCKLING RESTRAINED BRACE WITH FULL-LENGTH OUTER RESTRAINT: EXPERIMENT AND RESTORING FORCE MODEL

Bo Yang [1, 2], Zhan-Zhong Yin [1, *] and Hong-Bo Xu [1]

[1] *School of Civil Engineering, Lanzhou University of Technology, Lanzhou 730050, China*
[2] *Architecture and Civil Engineering Institute, Guangdong University of Petrochemical Technology, Maoming 525000, China*
** (Corresponding author: E-mail: yzztianyu@126.com)*

ABSTRACT

In order to solve the instabilities, fracture failures, and difficult repairs of welded gusset plates in buckling-restrained braced frames (BRBFs) under severe earthquakes, the idea of a full-length outer restraint BRB (FLBRB) is introduced. This new brace consists of a cross-section core, two end-weakened connectors, and a full-length outer restraint. In this paper, three FLBRBs with different parameters were designed, and their mechanical behaviors were evaluated through quasi-static testing, including failure mode, stress distribution and hysteretic behavior. Besides, the refined FE models were established and compared with the test. And the simplified bilinear load-displacement model and hysteretic rule considering the degradation of unloading stiffness are proposed based on the experimental investigation and FE simulation, the simplified bilinear load-displacement model and hysteretic rule considering the degradation of unloading stiffness are proposed, as well as the formulas for calculating the stiffness of either loading or unloading. The results demonstrate that the FLBRB has good hysteresis performance as it can confine the plastic to the weakened connectors and the BRB. Furthermore, the simplified restoring force model was verified by comparing it with the experiment, indicating that the load–displacement curve of the FLBRB could be accurately predicted by the suggested theoretical formula and model. These research results can be adopted to provide theoretical foundation for the engineering application of the FLBRB.

ARTICLE HISTORY

Received: 20 September 2022
Revised: 29 January 2023
Accepted: 18 February 2023

KEYWORDS

FLBRB;
Weakened connector;
Full length outer restraint;
Quasi-static test;
Hysteretic behavior;
Restoring force model

1. Introduction

As an traditional braced frame of structural steel, special concentrically braced frames (SCBFs) have higher bearing capacity, excellent ductility, and large lateral stiffness [1]. The connection between the frame and the brace are welded with gusset plate in the conventional design, and so the stress concentration is easy to generate in the joint field, which results in the brace being over-stressed and prematurely rupture at the welded corner gusset connection [2,3]. After a severe earthquake, such a permanently damaged brace and connection are very difficult to repair or replace, resulting in a structure not being able to restore its original form and function [4-6]. Although it is typical practice to design connections subjected to axial loads only, the yield of joints and the post-buckling response of braces should be balanced in the design process [7,8].

To address the aforementioned problems, researchers have made many improvements and conducted numerous studies. Fleischman et al. [9-12] applied cast modular components to beam-to-column connectors and nodes, compared with traditional connections, these designs exhibited superior energy dissipation and excellent ductility. De Oliveira et al. [13] proposed using high-strength connectors for connection of circular hollow sections in SCBFs, and connecting to the gusset plate by bolts or pins. Gary et al. [14] proposed the yielding brace system (YBS) for SCBFs. Through special design, the shear yielding elements at one end of the brace is designed for the inelastic energy dissipation under seismic loading in this system. Subsequently, the YBS has been further tested and developed [15,16]. Federico et al. [17] proposed a similar brace system called the floating brace (FB) system. This new concept creates a strong, rigid, and flexible lateral bracing system by using a series of special shaped plates at one end of a brace. On this basis, Ward et al. [18,19] designed a ductile bracing system according to the concept of “dog bone” [20], and introduced it to SCBFs. Through their theoretical and experimental research of system, they provided corresponding design methods and suggestions. Besides, Steven et al. [21] proposed an alternative connection of the concentrically braced frames. This connection can confine the damage to a replaceable module, while realizing rapid repair and replacement. Finally, Zhao et al. [22,23] proposed a new type of joint connection, which can effectively reducing the stress response at the joints of frame through the sliding of gusset plates.

According to the commentary of the code of AISC [24], the damage of SCBFs observed in previous severe earthquakes was generally caused by insufficient ductility and corresponding brittle failures of the connections. In addition, when the braces are compressed, they will buckle in advance, leading to instability or even failure of the structure during severe earthquake [5,25].

The researchers then proposed a buckling-restrained brace (BRB) and the improvement and optimization research were carried out. Wakabayashi [26] conducted an experimental study on BRB. Then, Watanabe et al. [27] developed a BRB consisting of steel core and concrete-filled steel tube, and it was verified by tension and compression tests that the BRB had excellent energy dissipation performance. Tsai et al. [28] proposed double-core configuration BRBs that reduce the length of the connecting section at the end of the BRB to improve the stability of the regions, and tested their hysteretic response experimentally. Jia et al. [29] conducted the quasi-static test on concrete composite frame with BRB, and proposed the design suggestions to improve the stability of BRB end connection.

For the BRBs is widely used in practical construction, the fabrication materials, yield behavior, assembly and connection types of BRBs were improved, including SMA BRBs, double-stage yield BRBs, and assembled self-centering BRBs [30-33]. The corresponding design methods were optimized [34-35]. As to enhance the performance of BRBs further, Yin [36] designed an improved double-tube BRB (IBRB), which set a series of contact rings between the inner tube and the outer tube to improve the mechanical properties of the double-tube BRB. Based on the advantages and good mechanical properties of IBRBs, the author applied it to the EBFs [37]. Furthermore, Yin developed a novel assembled BRB with ductile castings (CBRBs) [38,39], which solved the brittle failures of the gusset plates in the buckling restrained brace frames (BRBFs). By changing the details and design parameters of the CBRBs, the double-stage yield of the ductile castings and BRB was realized. This formed a repairable and replaceable structural system.

Based on the research achievements mentioned above, we have designed a new buckling-restrained brace with a full-length outer restraint (FLBRB), that consists of a cross-section core, end-weakened connector, and full-length outer restraint. The characteristics are as follows. The FLBRB is connected to the frame through weakened connectors using bolt connections to replace the traditional welded gusset plates. To avoid the brittle fractures and stress concentrations in the joint field and to confine the inelastic deformation on the end-weakened connectors, these connectors are repairable and replaceable after severe earthquakes. Using the full-length outer sleeve as the buckling restraint improves the stability of the end-weakened connector and avoids the instability of the connecting section between the weakened connector and core of BRB. Each part of the FLBRB is assembled with high-strength bolts on site, forming a structure in which all components can be repaired and replaced.

In this paper, three different parameters of FLBRB were tested under axial cyclic load. We analyzed its hysteretic behavior, developed the restoring force model of the FLBRB based on theoretical analysis, and verified the

experimental results. These results demonstrated that the FLBRB has stable hysteretic behavior, while the load-displacement curve calculated by the theoretical simplified bilinear model coincides fairly with the experimental results. The above conclusions are useful for further research of FLBRB in steel frame.

2. Design of the FLBRB

2.1. Description of proposed FLBRB

The FLBRB consists of the cross-section core, end-weakened connector, and full-length outer restraint, as shown in Fig. 1. Each component is fabricated in the shop and assembled by bolts on site, thus reducing the erection time. The weakened connectors can confine the plastic deformation to this part, which relieves the stress concentration at the beam-column joint, and effectively reduce the possibility of brittle fracture at the connection between the brace and the frame.

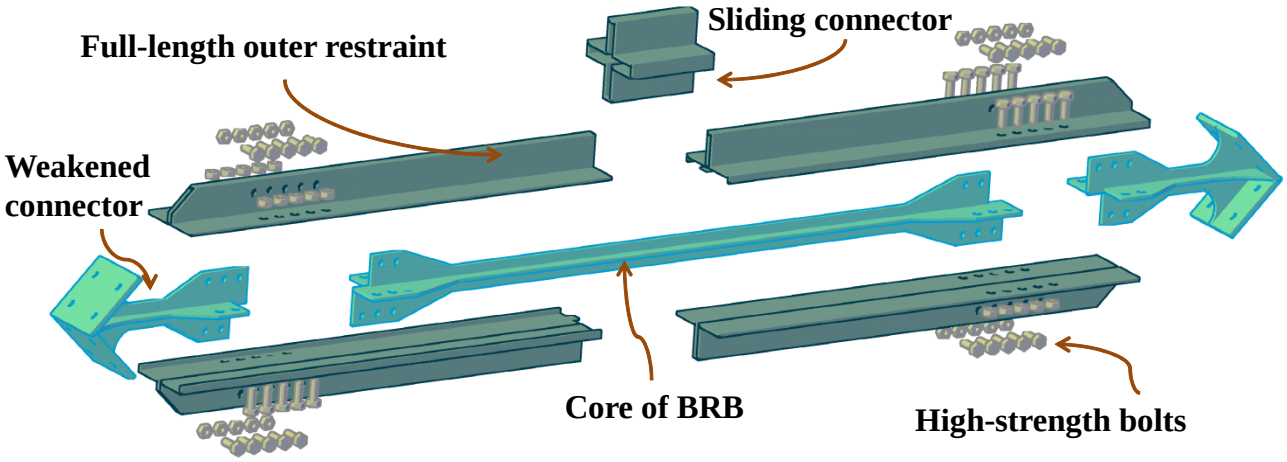

(a) Components

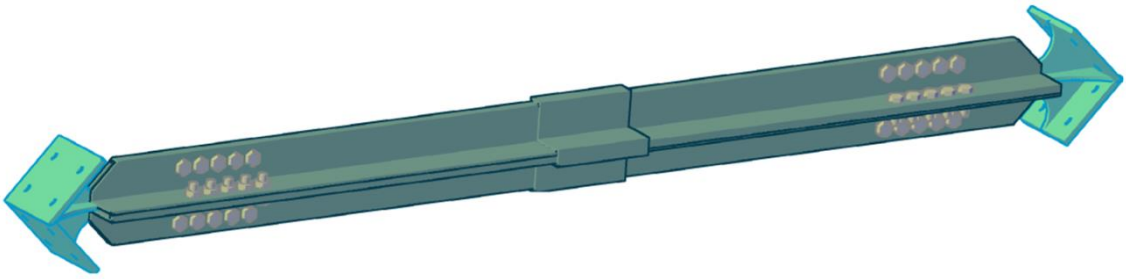

(b) Fabrication

Fig. 1 Example of a figure

2.2. Specimen design

An 11-story frame was used as a prototype. The planned dimensions are shown in Fig. 2(a). The structure was designed according to the relevant specifications, including the GB50011-2010 [40] and JGJ 99-2015 [41]. And the structure was scaled by 1/3 in consideration of the laboratory conditions.

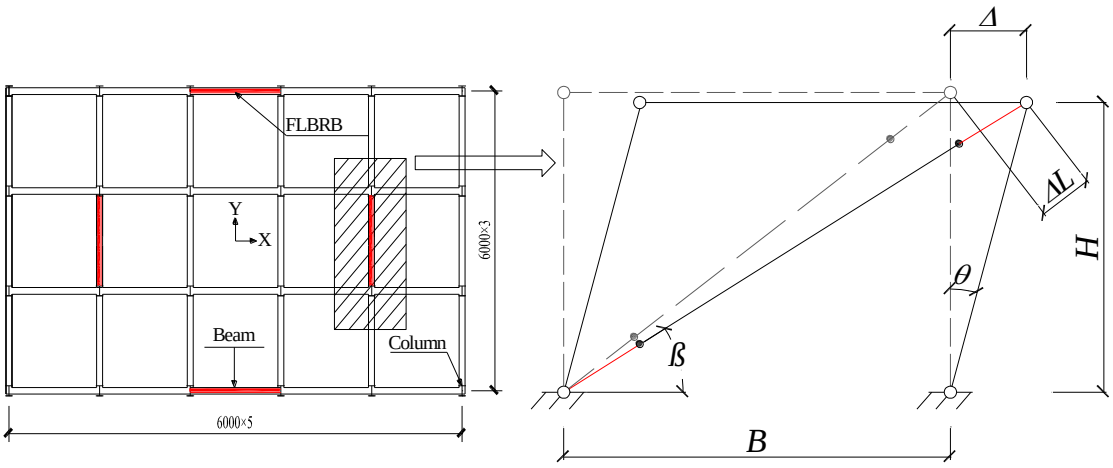

(a) Plane

(b) Schematic of one-story one-bay

Fig. 2 Schematic diagram of FLBRB frame

Fig. 2(b) gives a schematic diagram of one-story one-bay structure with FLBRB. The reasonable lateral stiffness distribution of the FLBRB and frame is an essential factor for the design of the structure. Prior to the research in this paper, the author completed the laboratory tests and numerical simulations of

the BRBFs with ductile castings (CBRBSFs). The research results showed that, when the lateral stiffness ratio is in a reasonable range [38], it is conducive to the performance of brace in CBRBFs and the maximum dissipation of seismic energy. Therefore, according to the recommended value and following steps to design:

(1) The column and beam are designed according to the design conditions including load and seismic intensity, etc. The horizontal stiffness of the frame is calculated by the following equation, which is called the D-value method:

$$K_F = 2\alpha \frac{12E_c I_c}{H^3} \tag{1}$$

where I_c and E_c are the cross-sectional moment of inertia and the Young's modulus of the column, respectively. H is the story height, α is a correction coefficient [42].

(2) Ignoring the change of the angle between the horizontal line and the FLBRB. (Fig. 2(b)). The lateral stiffness of the FLBRB is derived according to Eqs. (2) to (4):

The axial force of the FLBRB is:

$$\Delta L = \Delta \cos\beta = \frac{F\sqrt{B^2+H^2}}{E_B A_B} \Rightarrow F = \frac{E_B A_B \Delta \cos\beta}{\sqrt{B^2+H^2}} \tag{2}$$

The corresponding horizontal force of the FLBRB is:

$$F_x = F\cos\beta = \frac{E_B A_B \Delta \cos^2\beta}{\sqrt{B^2+H^2}} \tag{3}$$

The lateral stiffness of the FLBRB is:

$$K_B = F_x/\Delta = 2E_B A_B \cos^2\beta \sin\beta / H \tag{4}$$

where A_B is the cross-sectional area of the inner of FLBRB; β is the angle between the horizontal line and FLBRB; B is the span of the structure.

(3) By combining the above Eqs. (1) and (4), and defining the lateral stiffness ratio of FLBRB and frame (the recommended ratio k should be between 1.5 and 3.0), the cross-section of the FLBRB can be determined:

$$A = k \cdot K_F \cdot H / E_B \sin\beta \cos^2\beta \tag{5}$$

According to the previous the theoretical and experimental research [43,44], We found that three parameters had an obvious effect on the hysteretic performance, including the width-to-thickness ratios and the lengths of yielding segments of the weakened connectors, as well as the axial force ratio n:

$$n = p_W / p_B \tag{6}$$

where p_W and p_B are the axial tensile and compressive yield strength of the weakened connector and the core of BRB, respectively.

Thus, three FLBRB (termed FLBRB-1, FLBRB-2, and FLBRB-3) with different details (Table 1) were designed and conducted quasi-static tests. Due to limitations of test equipment and conditions, the length of a specimen is designed to be half of the original according to the principle of symmetry. The details and dimensions of the FLBRB are shown in Fig. 3. Including FLBRB-frame connection segment L_{c1}, yielding segment $L_{c2}(L_{c2'})$, transition segment $L_{c3}(L_{c3'})$, and weakened connector-BRB connection segment $L_{c4}(L_{c4'})$. The full-length sleeve as the outer restrained part is assembled by four equal angles steel, which can improve the stability at the connection between a weakened connector and BRB and restrain the buckling of the end-weakened connector [45].

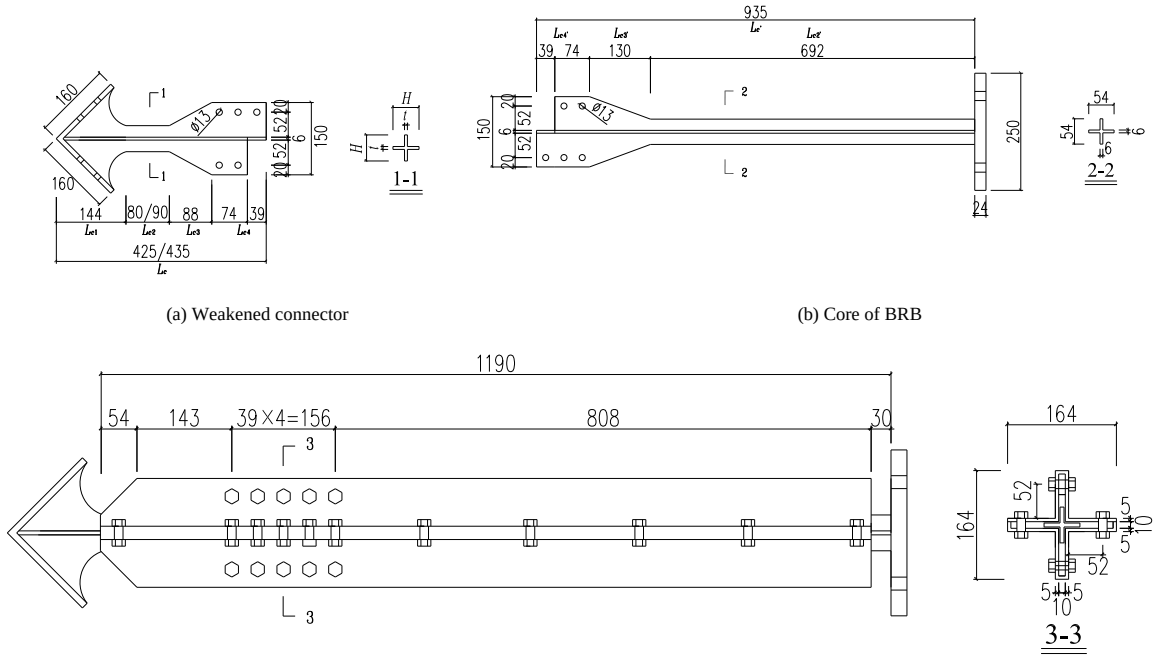

(a) Weakened connector

(b) Core of BRB

(c) FLBRB

Fig. 3 Schematic of FLBRB

Table 1
Parameters of weakened connector

Number of Specimens	Design Parameters						
	n	L_{c1}/mm	L_{c2}/mm	L_{c3}/mm	L_{c4}/mm	H/mm	t/mm
FLBRB-1	1.0	144	90	88	113	54	6
FLBRB-2	1.0		80			54	
FLBRB-3	0.8		90			43	

3. Experimental process

3.1. Coupon Tests

According to the test procedures recommended in the GB/T 228.1-2010 [46] and GB/T 2975-2018 [47]. Standard plate tensile coupons were prepared (Fig. 4) to test the steel properties, which are listed in Table 2 below.

Fig. 4 Coupon test of specimens

Table 2
Properties of steel

Specimen	Yield strength f_y/Mpa	Ultimate strength f_u/MPa	Young's modulus E/MPa	Elongation δ/%
Weakened connector	237	424	232800	26
Core of BRB	240	450	220000	25
Full length outer restraint	340	500	210500	26

3.2. Loading device and protocol

The test was conducted in the western engineering research center. The maximum output load of the vertical loading device was 2000 kN. The device consisted of a vertical loading frame and concrete reaction floor, equipped with an electro-hydraulic jack, a rigid base, and a right-angle support simulating the connection of the beam-column joint. The rigid base and right-angle support were fixed by high-strength bolts of d = 20mm. And the surrounding of the electro-hydraulic jack was restrained by the scaffolds to prevent non-axial displacement during loading, as shown in Fig. 5.

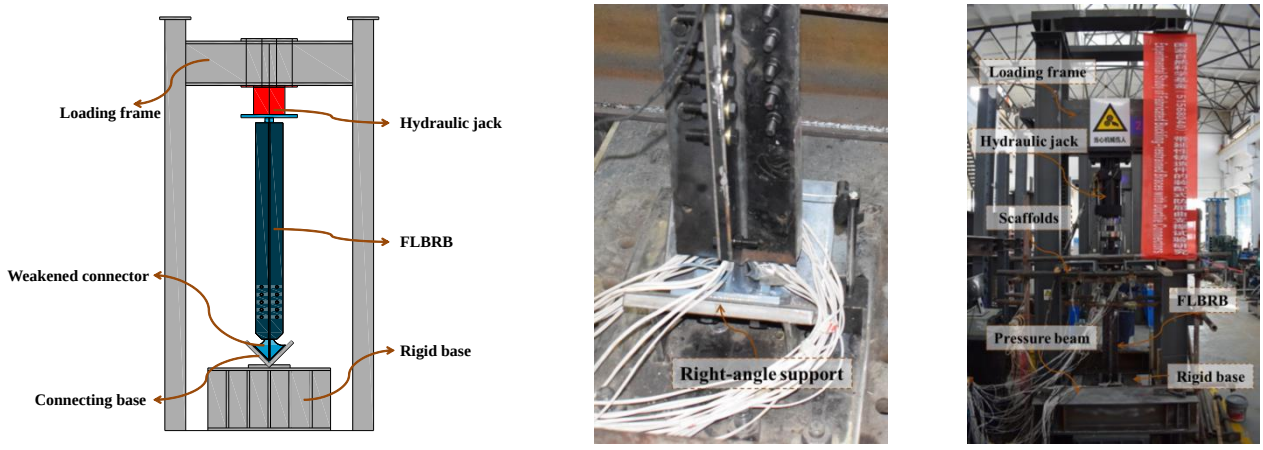

(a) Details of vertical loading device (b) Connecting base (c) On-site

Fig. 5 Loading device

The displacement loading control recommended by the specification [48] was implemented in this test. Fig. 6 showed the amplitudes of the loading, which were 1mm, 3mm and 5mm …. The test would be stopped until the specimen was damaged.

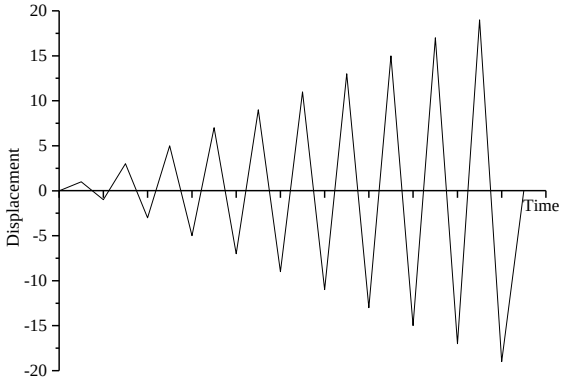

Fig. 6 Loading Protocol

3.3. Layout of measuring point

Fig. 7(a) shows the arrangements of displacement meters. Since the test adopted vertical loading, the axial deformation of FLBRB and weakening connector was measured by No. 1 and No. 2, respectively. In addition, considering the possibility of non-axial deformations of FLBRB, the Nos.2 to No.4 were arranged for measurement. And the arrangements of strain-gauge of FLBRB are illustrated in Fig. 7(b).

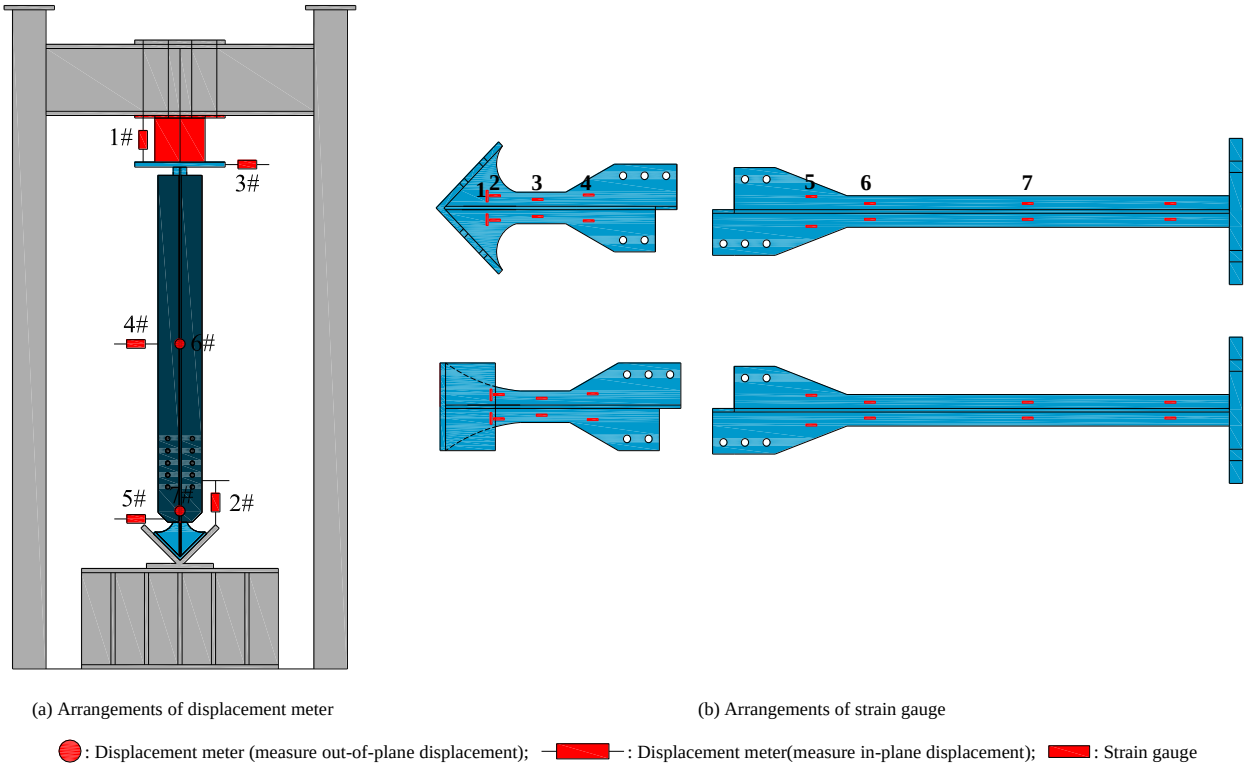

(a) Arrangements of displacement meter

(b) Arrangements of strain gauge

Fig. 7 Test point layout

3.4. Test description

The following rules were established: (1) Before the test, preloading was required to test the device as well as eliminate the installation gap of specimen; (2) Loading directions were downward positive and upward negative; and (3) θ was defined as the story drift angle of the corresponding structure with FLBRB.

Under cyclic loading, no obvious experimental phenomenon was observed before 3 mm loading displacement ($\theta=1/210$), and three specimens were in the elastic stage. Starting from 5 mm ($\theta=1/125$), closer inspection of readings of the No. 2 displacement meter showed that the connection between the weakened connector and BRB of FLBRB-1 slipped for a displacement of approximately 2 mm in the axial direction, which was also observed in the other specimens. Continuing the loading, it was found that the data of No. 1 and No. 2 displacement meters increased with the increasing test load, indicating that the weakened connector and core of BRB begin to deform in axial compression and tension. As the loading displacement approaching 7 mm ($\theta=1/90$), the yielding segment of the weakened connector reached the yield first. Further comparisons of data of displacement meters and strain gauges indicated that the elongation and compression of a weakened connector are larger than those of core of BRB. Moreover, the friction sound of the specimen was heard, and this was due to the friction between the weakened connector and the inner of the full-length outer restraint, resulting in the compression load of the specimen being greater than the tensile load.

When the loading displacement was close to 13 mm ($\theta=1/50$), the reading of Nos. 4 to 7 displacement meters changed slightly, and the core of the BRB entered the elastic-plastic stage and twisted. Subsequently, it was observed that the readings of the No. 1 and No. 2 displacement meters differed by more than 3mm, and this was attributed to the increased bolts slipping at the connection of the weakened connector and BRB. With the further increase of the loading, the friction between the weakened connector and the outer restraint intensified, resulting in the failure of some strain gauges, and the core-high-order buckling began to appear at the displacement of 17 mm ($\theta=1/40$). When the displacement finally loaded to 19 mm ($\theta=1/35$), the loading-carrying capacity of FLBRB-1 and FLBRB-2 reached the peak value, while that of FLBRB-3 began to dropped, thus the test was stopped.

3.5. Stress responses

The stress of each measuring point of the FLBRB in Fig. 7(b) was analyzed in the following description when the axial deformation of the specimen was 3mm, 7mm, 13mm and 19mm, respectively.

A significant difference among the stress responses of the three specimens was not evident. For simplicity, we took the stress data of FLBRB-1 as an example to illustrate the main characteristics of the stress distribution. As shown in Fig. 8(a), at the loading displacement of 3 mm ($\theta=1/210$), the stress of each measuring point was small. When the axial deformation increased to 7 mm ($\theta=1/90$), the stress at points Nos. 1 to 4 of the weakened connector was 132.0 MPa, 223.8 MPa, 243.6 MPa, and 237.9 MPa, respectively, which approached or exceeded the yield stress. This indicated that the weakened connector began to yield and resulted in yielding deformation, while the core of the BRB remained an elastic state, which the maximum stress response was only 168.3 MPa. As the test continued, the stress responses of the BRB and weakened connector rose with loading. When the axial deformation climbed to 13 mm ($\theta=1/50$), the stress responses of Nos. 1 to 4 were 253.2 MPa, 301.1 MPa, 323.6 MPa, and 302.4 MPa, respectively, while the maximum stress responses of Nos. 5 to 7 was 264.1 MPa. This result revealed that the plastic deformation appeared in BRB, which dissipated seismic energy with the weakened connector. It is noteworthy that the stress responses of the weakened connector (points Nos. 1 to 4) were greater than that of the core of the BRB (points Nos. 5 to 7) during the test process, as shown in Fig. 8. These results sufficiently demonstrate that the weakened connector began to yield before the BRB supplemented the energy dissipation. More importantly, the above stress responses and yield processes also satisfy the performance requirements of elastic and elastic-plastic story drift angle limited value ($\theta=1/250$ and $\theta=1/50$) recommended by the GB50011–2010.

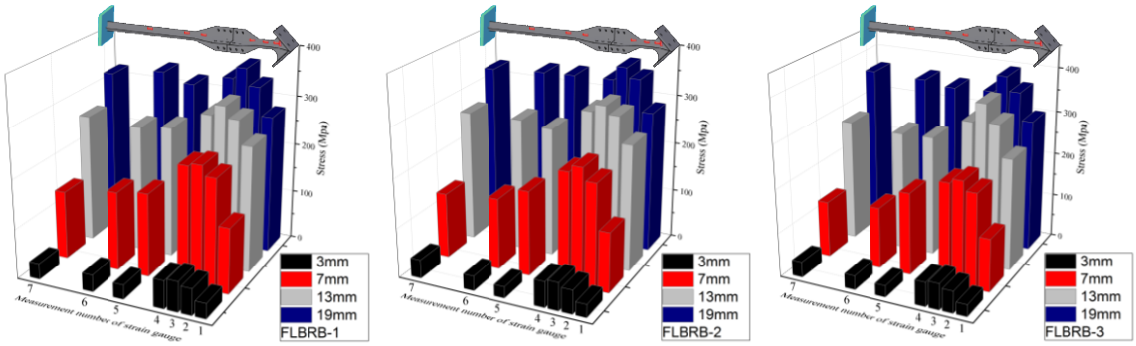

(a) FLBRB-1 (b) FLBRB-2 (c) FLBRB-3

Fig. 8 Comparison of stress responses of weakened connector and core of BRB

3.6. Failure process

The loading phenomenon and failure mode of the three specimens showing a basically consistent process during the test. At the loading level of 3 mm ($\theta=1/210$), three specimens were kept in elastic. When the axial deformation was increased to 7 mm ($\theta=1/90$), note that the strain of the weakened connector exceeded the yielding strain and had enter the plastic stage. As the axial displacement approached 13 mm ($\theta=1/50$), the stress of the core of BRB showed that it also yielded to consume energy. When the displacement expanded to 17 mm ($\theta=1/40$), the core-high-order buckling phenomenon occurred at the FLBRB, as shown in Fig. 9. Finally, the BRB and the weakened connector showed excessive deformation under axial cyclic load, especially in the FLBEB-3, for which the failure mode belongs to the fracturing due to the obvious deformation and buckling of the weakened connector. The main reason is that the smaller axial force ratio lead to premature buckling and fatigue failure at the yielding segment of the weakened connector under cyclic load. In summary, the failure process of the three specimens were ductile failures.

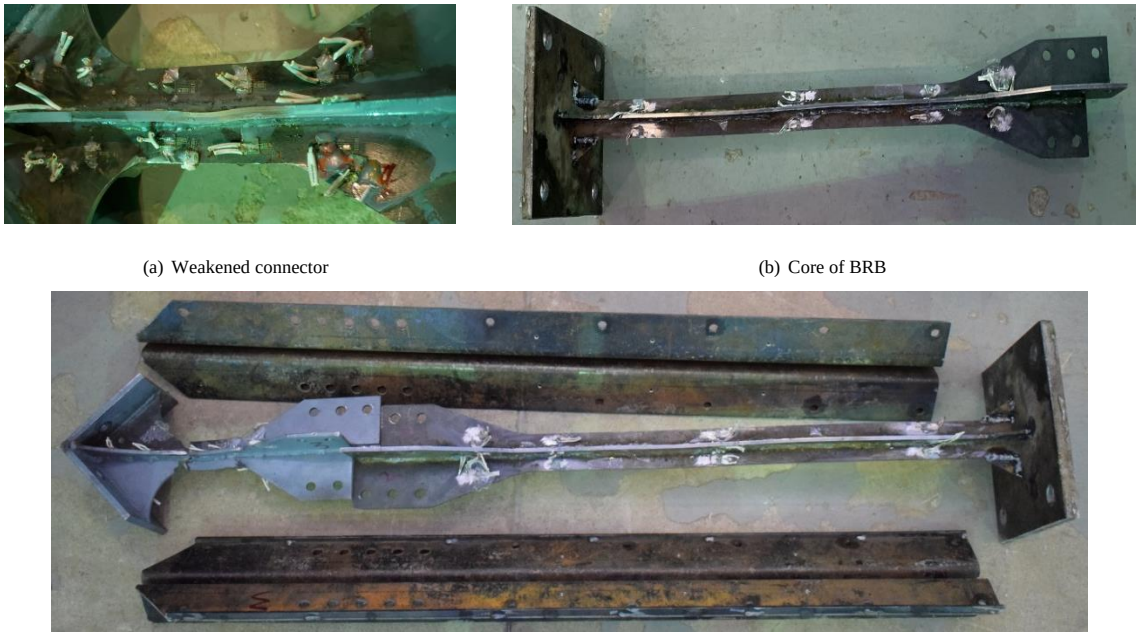

(a) Weakened connector (b) Core of BRB

(c) Disassemble the specimen

Fig. 9 Deformation of specimen

3.7. Hysteretic curve

The hysteretic curves of FLBRB-1, FLBRB-2, and FLBRB-3 are presented in Fig. 10. The load-displacement loops of three specimens had a shape of spindle and stable hysteretic capacity without obvious degradation during the loading process. The energy dissipation coefficient *E* of FLBRB-1, FLBRB-2, and FLBRB-3 were 2.38, 2.44, and 2.09, respectively, which verified that the FLBRB can effectively dissipate energy under cyclic load, and has excellent seismic behavior. What stood out in data from FLBRB-1 and FLBRB-2 was the coefficient *E* decreased with an increase in the length of the yielding segment of the weakened connector. These conclusions are consistent with the calculation of the total area of hysteretic curves.

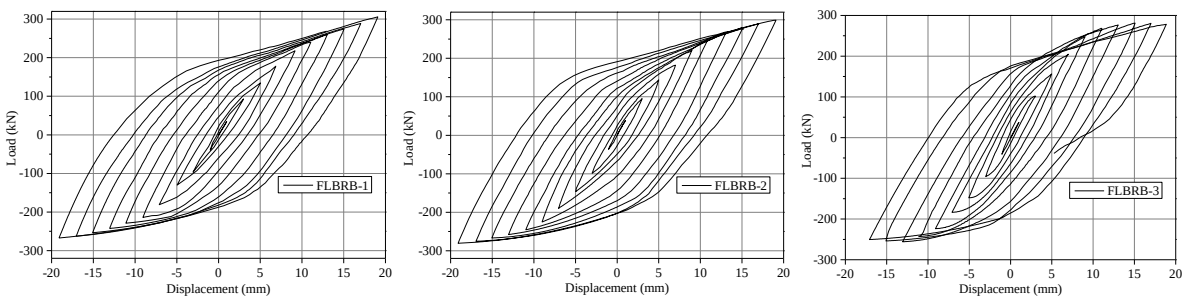

Fig. 10 Hysteretic Behavior of the FLBRB

The load-displacement curves of all specimens were similar and displayed a narrow shape during the initial stage. With the test progressed, it was observed that the area surrounded by the curve gradually increased with a increase of loading-carrying capacity, indicating that the weakening connector began to enter the phase of elastic-plastic, and the plastic energy consumption of the specimens increased steadily. When the loading reached a certain stage, another noteworthy finding was that the asymmetry between the compression and tension loading deteriorated as the friction interaction between the core of FLBRB and the inner surface of the full-length outer restraint increased.

In the later phase of the test, the loading of the specimens increased slowly and gradually achieved peak. Remarkably, the load of FLBRB-3 with the minimum axial force ratio declined significantly due to premature failure. The main cause of this result was that the axial force ratio reduced to a certain value that caused the weakened connector to become a weak component during the late stage of the experiment, which was not conducive to the energy consumption of the FLBRB. Consequently, the optimal axial force ratio was recommended in the range of 0.9 to 1.0 to ensure the bearing and hysteretic capacity of the specimen.

3.8. Skeleton curve

Fig. 11 shows skeleton curves of specimens, and related key parameters of the skeleton curves are presented in Table 3.

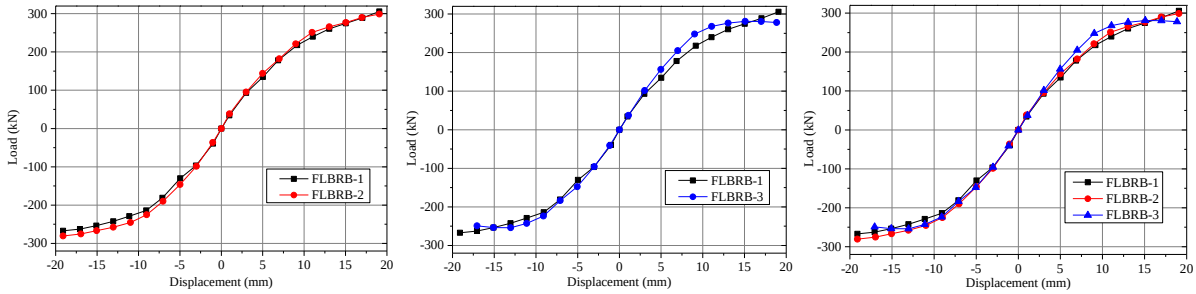

Fig. 11 Comparison of skeleton curves

A similar variation trend and loading-carrying capacity were observed from the comparison of skeleton curves. All specimens remain elastic within an axial displacement of approximately 5 mm. The initial stiffness in the positive and the negative increased linearly. Notably, the initial stiffness of FLBRB-2 was greater than that of the FLBRB-1, showing that the FLBRB-2 has higher yield load. With the progress of the test, the load increased at a slower speed and the slope of the curve decreased gradually.

For FLBRB-1 and FLBRB-3, the stiffness of FLBRB-3 degraded seriously at the later phase of test, and the ultimate strength of FLBRB-3, which has a low axial force ratio, is dramatically lower than that of FLBRB-1. This consequence further confirms the relationship between the loading-carrying capacity and axial force ratio; that is, the low axial force corresponds to a worsening energy dissipation and plasticity of the yielding segment of the weakened connector. In addition, the process of decreasing the length of the yielding segment of weakened connector is conducive to increasing the plasticity of the weakened connector and the loading-carrying capacity of the FLBRB.

4. Numerical simulation

4.1. FE modeling

Numerical simulation using Abaqus/Standard (version 6.12) was performed to investigate the yield mode and cyclic behavior of three specimens. Nonlinear material properties (Table 2) with the isotropic-kinematic hardening rules were implemented to reproduce the plastic behavior of all models.

The initial imperfection of 0.1% of the FLRBR length was imposed on the model. And the algorithm of Newton-Raphson was utilized for large displacement analyses. Besides, the 3D modeling was established using eight-node reduced integration solid element (C3D8R). And the element mesh sizes of the core of FLBRB and the full-length outer sleeve were 10 mm, and 20 mm, respectively (Fig. 12). Considering the interaction between the core of the FLBRB and the outer restraint, the hard contact and the penalty method were used for calculation of perpendicular and tangential interaction between inner and outer of the FLBRB, respectively. Applied the fixed constraint to the connection-end of the FLBRB, and the horizontal loading consistent with the test was applied at the reference point on the right side of the FLBRB, as shown in Fig. 13.

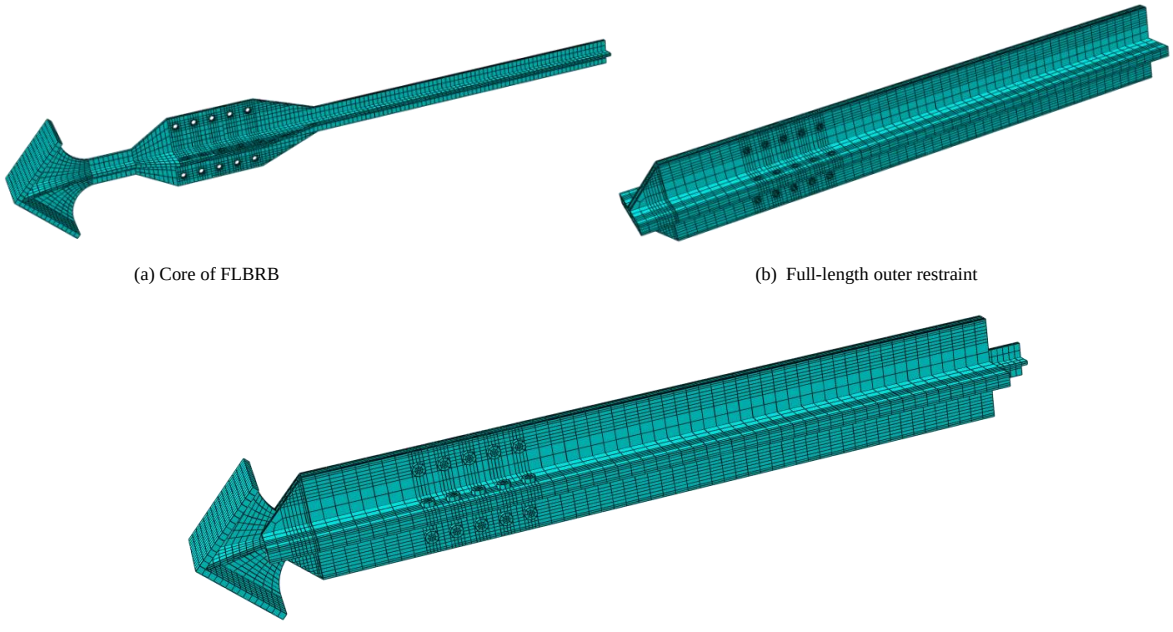

(a) Core of FLBRB

(b) Full-length outer restraint

(c) FLBRB

Fig. 12 FE model

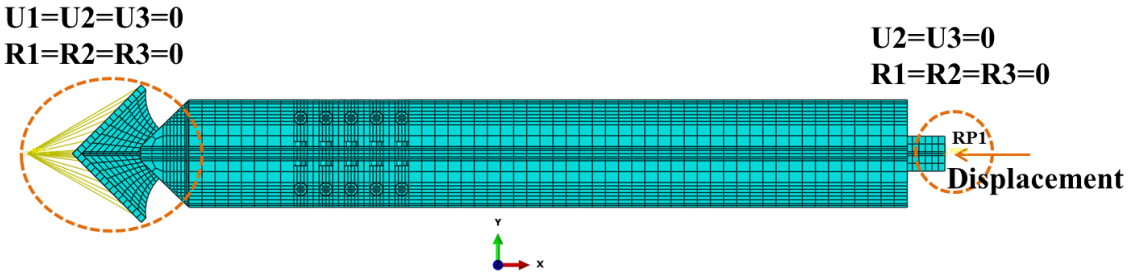

Fig. 13 Boundary constraints of FE model

4.2. Model verification

The hysteretic curve obtained from the FE of the FLBRB is shown in Fig. 14, displaying overall satisfaction between the FE and the test results. Besides, the numerical model can simulate the tension-compression asymmetric behavior well, and the maximum compression capacity is approximately larger than the maximum tension capacity by 10%. Furthermore, the prediction error of the ultimate bearing capacity was mostly less than 10% and some even within 1%, thus showing the accuracy of the refined FE model. However, there is a large error in the initial stiffness at the initial stage for the three specimens as depicted in Table 3. One of the prime reasons for the higher deviation of elastic stiffness was that the inevitable installation clearance and slipping in bolted connection resulting in inaccurate measurements of axial displacements. Nevertheless, the energy dissipation coefficients E of the experimental and FE models were both exceed 2.0, which indicated that the FLBRB has excellent energy dissipation capacity.

The stress distributions of the FLBRB with axis displacements of 3 mm, 7 mm, 13 mm, and 19 mm obtained from the FE simulation are shown in Fig. 15. Comparing with the stress response in Fig. 8 reveals that the stress value obtained from the FE simulation is consistent with the test at different loading displacements. At the initial loading stage, a weakened connector enters the plastic stage before BRB. With the test proceeding, both of BRB and weakened connector dissipate energy through plastic deformation. According to Mises stress diagram, it can be seen that the maximum stress of the FLBRB is mainly confined to the weakened connector.

As shown in Fig. 16, the similar deformation was observed in the comparison results. In addition, the failure regions of the specimens were coincident with the locations in the FE model. High-order buckling in core of BRB was well captured. In conclusion, the refined FE model provided an effective prediction for the dissipated energy, asymmetry behavior and buckling shape of the FLBRB under cyclic loading. Accordingly, the further theoretical research on FLBRB can be investigated through the FE simulated results.

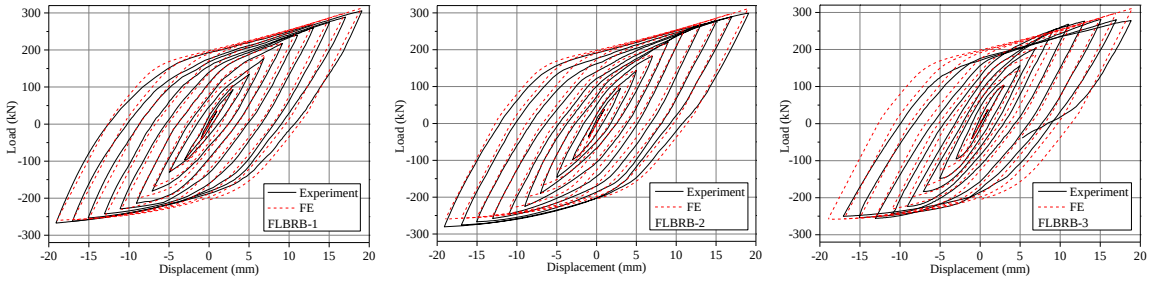

Fig. 14 Comparison of FE and experiment

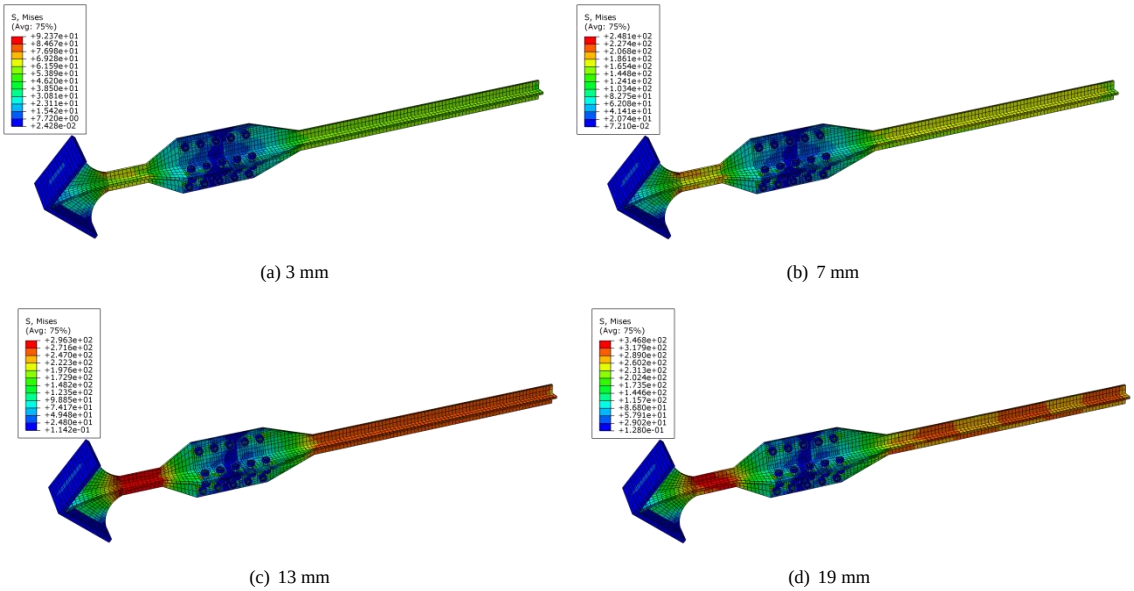

(a) 3 mm (b) 7 mm

(c) 13 mm (d) 19 mm

Fig. 15 Stress distribution of the FLBRB with different loading displacement

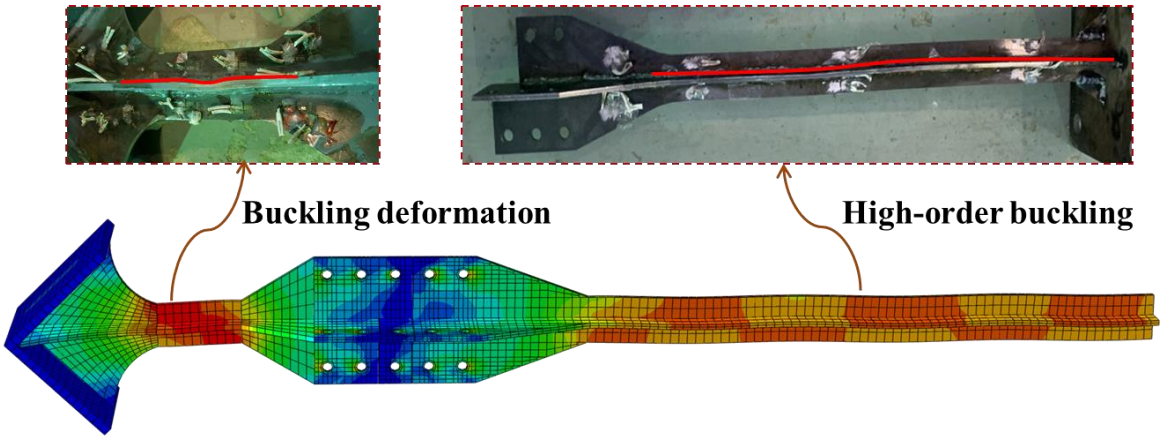

Fig. 16 Comparison of deformation

Table 3
Comparison of analysis results

			Positive		Negative	
			K_0 (kN/mm)	P_{max} (kN)	K_0 (kN/mm)	P_{max} (kN)
FLBRB-1		Test	38.68	305.664	38.5	-267.312
		FE	41.72	312.61	41.69	-260.39
		Theory	42.27	318.06	42.27	-289.14
	Error	Test-FE	7.29%	2.22%	7.65%	3.08%
		Theory-FE	1.3%	1.71%	1.37%	9.94%
		Theory-Test	8.49%	3.90%	8.92%	7.55%
FLBRB -2		Test	39.55	298.85	40.62	-280.61
		FE	42.1	311.23	42.08	-260.96
		Theory	42.48	318.86	42.48	-289.87
	Error	Test-FE	6.06%	3.98%	3.47%	7.86%
		Theory-FE	0.89%	2.39%	0.94%	9.97%
		Theory-Test	6.9%	6.28%	4.38%	3.19%
FLBRB -3		Test	37.46	281.09	38.62	-254.2
		FE	40.13	311.23	41.06	-258.56
		Theory	41.16	309.74	41.16	-281.58
	Error	Test-FE	6.65%	9.68%	5.94%	1.69%
		Theory-FE	2.5%	0.48%	0.24%	8.18%
		Theory-Test	8.99%	9.25%	6.17%	9.72%

5. Restoring force model of FLBRB

Based on the above tests and referring to the research of FLBRBs [44], the bilinear mechanical model for FLBRB was proposed through theoretical analysis, as well as the calculation for the stiffness of either loading or unloading was formulated. And the restoring force model of the FLBRB was proposed by combining the bilinear skeleton curve model and the load-unload rule, which is a reasonable calculation method for the further research of the design of a structure with FLBRB.

5.1. Bilinear mechanical model

Based on the experimental results, the axial displacement and loading-carrying capacity curve of the FLBRB can be simplified by a bilinear model. By analyzing the changing trend of the skeleton curve, it can be divided into two phases (Fig. 17) .

Phase I (Elastic stage, OA/OA'): In this stage, the whole specimen remains elastic. The load-displacement relationship changed linearly, which implies that the slope of the curve is equal to the initial stiffness of the FLBRB numerically.

Phase II (Elastic-plastic stage, AB/A'B'): The specimen enters this stage after reaching the yielding load. With the increase of displacement, the growth of load is slower than that of the Phase I, displaying obvious stiffness degradation characteristic, which is mainly caused by the yielding of the weakened connector and the BRB.

Accordingly, the simplified bilinear mechanical model needs to determine six characteristic parameters: initial stiffness K_y, yield displacement Δ_y, yield load P_y, post yield stiffness K_p, ultimate load P_u, and ultimate displacement Δ_u.

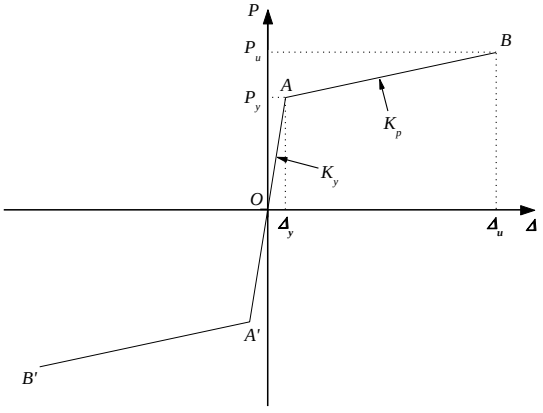

Fig. 17 Simplified Bilinear Mechanical Model

Initial stiffness K_y :

During the FLBRB design process, the equivalent stiffness is proposed to determine the initial stiffness of the specimen, which consists of weakened connector stiffness and BRB stiffness. The following Eqs. (7)-(9) were used to calculate the initial stiffness of the FLBRB based on series mechanism.

$$K_y = \frac{1}{1/K_{WC} + 1/K_{BRB}} \tag{7}$$

where K_{WC} and K_{BRB} are the elastic stiffness of the weakened connector and the BRB, respectively.

The elastic stiffness of the weakened connector K_{WC} can be obtained by Eq. (8), in which $K_{L_{c1}}$, $K_{L_{c2}}$, $K_{L_{c3}}$,and $K_{L_{c4}}$ are the stiffness of corresponding segments of L_{c1}, L_{c2}, L_{c3} and L_{c4} (as shown in Fig. 3(a)).

$$K_{WC} = \frac{1}{1/K_{L_{c1}} + 1/K_{L_{c2}} + 1/K_{L_{c3}} + 1/K_{L_{c4}}} \tag{8}$$

Similarly, elastic stiffness of the BRB can be calculated by the Eq. (9):

$$K_{BRB} = \frac{1}{1/K_{L_{c2'}} + 1/K_{L_{c3'}} + 1/K_{L_{c4'}}} \tag{9}$$

where $K_{L_{c2'}}$, $K_{L_{c3'}}$ and $K_{L_{c4'}}$ are the stiffness of corresponding segments of $L_{c2'}$, $L_{c3'}$ and $L_{c4'}$ for the core of BRB, respectively(Fig. 2(b)).

The stiffness in above Eqs. (7)-(9) can be calculated using axial stiffness formula $K = EA / L$.

Yield displacement Δ_y :

Based on the design concept of the FLBRB, the yield displacement of the FLBRB is determined by:

$$\Delta_y = \Delta_{WC,y} + \Delta_{BRB,y} = \frac{N_{WC} L_{WC}}{EA_{WC}} + \frac{N_{BRB} L_{BRB}}{EA_{BRB}} \tag{10}$$

where N_{WC} , N_{BRB}, A_{WC}, A_{BRB}, L_{WC} and L_{BRB} are the axial force, core cross-sectional area and length of the weakened connector and the BRB, respectively.

Yield load P_y :

When the FLBRB yields, the yield load is calculated according to the following equation:

$$P_y = K_y \cdot \Delta_y \tag{11}$$

Ultimate load P_u :

The strain hardening and the frictional interaction between the core of the FLBRB and the inner surface of the full-length outer restraint should be considered when calculating the ultimate load of the FLBRB, which is proposed by following Eq. (12):

$$P_u = \omega \cdot \gamma \cdot P_y \tag{12}$$

where ω is the strengthening factor of steel. According to the tests of three specimens and specified value in JGJ 99-2015, the recommended value for the Q235B steel is larger than 1.5. γ is the ratio of the maximum compression bearing capacity of the FLBRB to the maximum tensile bearing capacity. The AISC 341-16 specifies that the factor (γ) should be less than 1.3.

Ultimate displacement Δ_u :

Introducing the FLBRB incorporated into the SCBFs, the yield mechanism of the structure assumed that when the story drift angle of structure reaches the limit value specified in the GB50011-2010, the FLBRB forms a ductile failure mechanism. Ignores the deformation of the frame itself, the ultimate displacement of the FLBRB caused by the horizontal displacement of the structure can be expressed as:

$$\Delta_u = tg\theta \frac{BH}{L} \tag{13}$$

where L is the design length of FLBRB; θ is the ultimate story drift angle of the frame.

Post yield stiffness K_p :

The end weakening connector and BRB enter the elastoplastic stage successively, when the FLBRB exceeds the elastic stage. The post yield stiffness of the FLBRB can be calculated according to the following Eq. (14):

$$K_p = \frac{P_u - P_y}{\Delta_u - \Delta_y} \tag{14}$$

5.2. Bilinear mechanical model

The characteristic points of the bilinear mechanical model can be calculated according to Eqs. (7)-(14). The comparison of the theoretical skeleton curve and the test results is shown in Fig. 18 and Table 3. And there were differences of 8.71%, 5.64% and 7.58% between the theoretical initial stiffness (K_y) and the experimental initial average stiffness for three specimens, respectively, while the computed ultimate load (P_u) of the FLBRB agreed well with the tested ultimate load within a 10% difference. The result of having a larger difference in initial stiffness was possibly because of the installation clearance and slippage in the bolted connection and the discreteness of the test data. Meanwhile, the results showed the theoretical initial stiffness and ultimate load of the three specimens can be well fitted with the test, with an average difference of 7.31% and 6.65%, respectively. The results of comparison and analysis confirmed that the suggested Eqs. (7)-(14) can be used to calculate the equivalent stiffness and bearing capacity of the FLBRB.

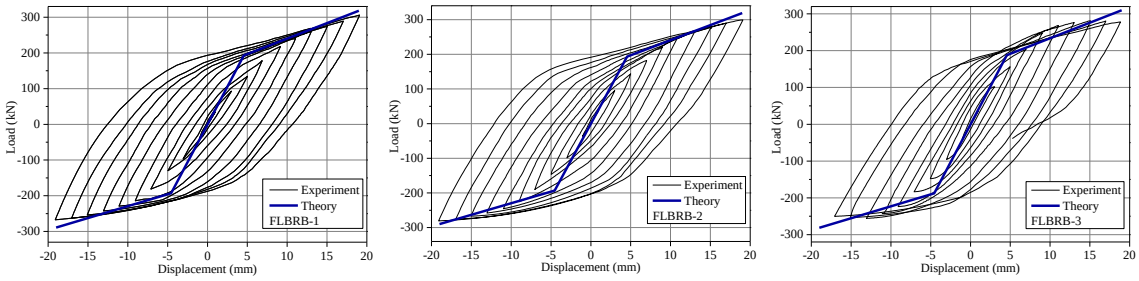

Fig. 18 Verification of the simplified bilinear mechanical model

5.3. Simplified restoring force model

On the basis of the theoretical analysis and numerical regression of FE data, the simplified restoring force model was established. According to the hysteretic curves of test, the loading phase can be divided into four typical stages: positive elasticity, positive elastic-plasticity, negative elasticity, and negative elastic-plasticity, while the unloading phase is divided into two typical stages: positive unloading and reverse unloading. Fig. 19 depicts the proposed restoring force model of the FLBRB. And the hysteresis criterion can be concluded as follows:

(1) When the loading does not reach the yield displacement Δ_y, the FLBRB is in the elastic stage, *OAB* and *OA'B'* are the positive and negative loading-unloading routes of the specimens, and K_y represents the loading and unloading stiffness. The bearing capacity was symmetrical on the whole in positive and negative loading directions.

(2) The loading route process along with the skeleton curves when the

loading exceeds the yielding load from the yielding point *A* to the *a*, the stiffness can be defined as post yield stiffness K_p. Then the unloading process reaches the point *b*, the slope of *ab* is defined as the positive unloading stiffness K_1. After that, the specimen continues reverse loading along the route *bA'c*, then unloads from point *c* towards point *d*, and the slope of *cd* is defined as the negative unloading stiffness K_2. Then continue to load and cycle until the maximum displacement.

(3) As the load over the yield load of the FLBRB, the unloading stiffness will gradually decrease with the increasing load due to the weakened connector and core of BRB yield successively. As shown in Fig. 20, fitting unloading stiffness data for each hysteretic loop to obtain the K_1 and K_2:

$$K_1 = 0.93218K_y(\Delta_1/\Delta_u)^{-0.0393} \tag{15}$$

$$K_2 = 0.90856K_y(\Delta_2/\Delta_u)^{-0.0319} \tag{16}$$

where Δ_1 and Δ_2 are the displacement corresponding to the positive and negative unloading, respectively.

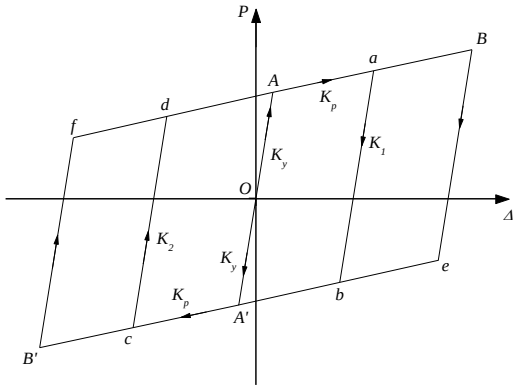

Fig. 19 Simplified restoring force model

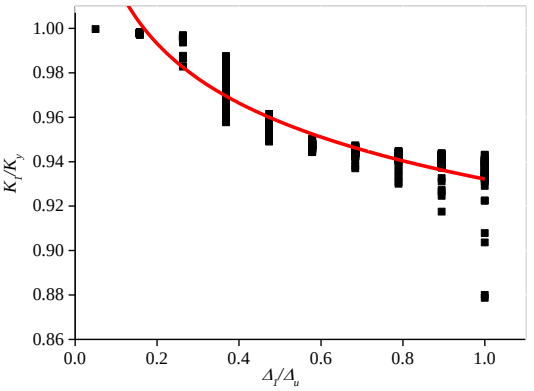

(a) Positive

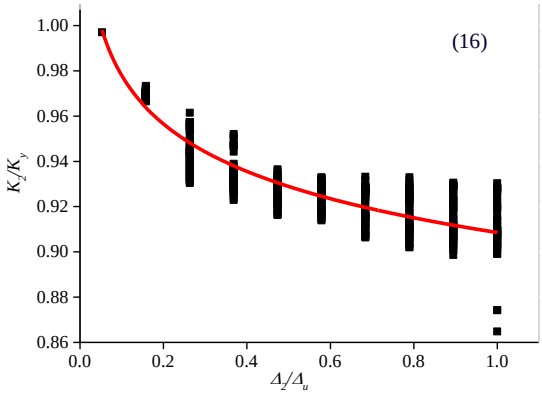

(b) Negative

Fig. 20 Fitting curve of stiffness degradation

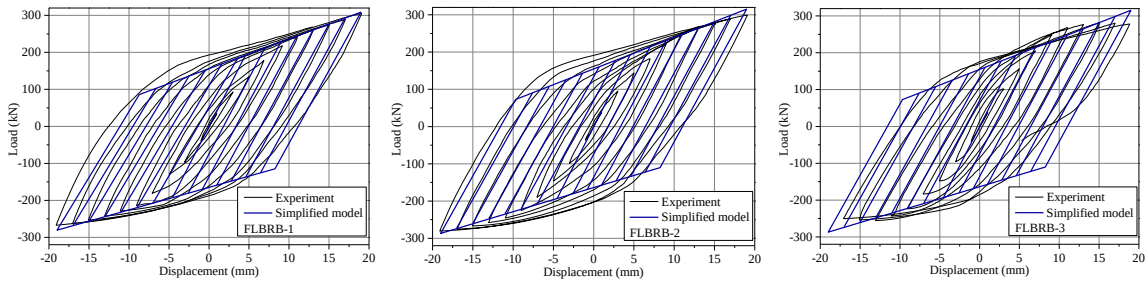

Fig. 21 Verification of restoring force model

5.4. Validation of theoretical model

To verify the theoretical restoring force model, the experimental hysteretic curves of three specimens are comparted with the calculated model, as shown in Fig. 21. A satisfactory agreement of hysteretic behaviors between the theoretical model and test results was observed, which shows that the suggested loading-unloading rule can predict the hysteresis behavior of the FLBRB. However, it can be found that the theoretical restoring force curve does not transit smoothly, mainly attributed to the simplified bilinear mechanical model adopted by the skeleton curve.

6. Conclusion

The new assembled buckling-restrained brace with a full-length outer restraint (FLBRB) was designed and tested to evaluate its hysteretic properties. The experimental results and comparisons of the test with numerical analysis were analyzed. In addition, a theoretical restoring force model was established and verified with experiments. Conclusions are listed below:

(1) The FLBRB showed excellent hysteretic property and deformation ability. The inelastic deformation was mainly concentrated in the weakened connector and BRB using the full-length outer restraint, which effectively improves the stability of the end-weakened connector and avoids the instability of the connecting section between the weakened connector and the BRB.

(2) The specimen with a bolted connection was convenient for installation and replacement. Each part of the FLBRB is assembled with high-strength bolts on site, forming a structure in which all components can be repaired and replaced.

(3) The numerical models of specimens were established, and the dissipated energy, asymmetry behavior and buckling shape of the FLBRB were verified by the tests. The result indicated that the refined FE model can simulate the behavior of the FLBRB under cyclic load well.

(4) On the basis of equivalent stiffness, a formula of the simplified bilinear skeleton model and the load-unload criterion was proposed and validated numerically and experimentally, which can be used to predict the hysteretic curve of FLBRB.

(5) The experimental and theoretical research will provide the suggestion and reference for designs and applications of the FLBRBs in the structures of buildings. Besides, further numerical simulation and test are needed to study the mechanical behaviors and the seismic performances of the structure with the FLBRB.

Acknowledgments

This study has been supported by the National Natural Science Fund of

China under grant No. 51968044, and the National Key Research and Development Program of China No. 2019YFD1101003.

References

[1] Uriz P., "Toward earthquake-resistant design of concentrically braced steel frame structures", PhD Thesis, University of California, Berkeley, CA, USA, 2005.

[2] Astaneh-Asl A., Goel S.C., and Hanson R.D., "Cyclic behavior of double angle bracing members with end gusset plates", Research Report UMEE 8287, University of Michigan, Ann Arbor, MI, USA, 1989.

[3] El-Tayem A.A., and Goel S.C., "Cyclic behavior of angle X - Bracing with welded connections", Research report UMCE 85-4, University of Michigan, Ann Arbor, MI, USA, 1985.

[4] Black R.G., Wenger W.A.B., and Popov E.P., "Inelastic buckling of steel struts under cyclic load reversals", UCB/EERC-80/40, Earthquake Engineering Research Center, University of California, Berkeley, CA, USA, 1980.

[5] Tremblay R., Filiatraul A., and Timler P., "Performance of steel structures during the 1994 Northridge earthquake", Canadian Journal of Civil Engineering, 22(2):338-360, 1995.

[6] Hsiao P.C., "Seismic Performance Evaluation of Concentrically Braced Frames", PhD Thesis, University of Washington, Seattle, WA, USA, 2012.

[7] Roeder C.W., Lehman D.E., Clark K., Powell J., Yoo J.H., Tsai K.C., Lin C.H., and Wei C.Y., "Influence of gusset plate connection and braces on the seismic performance of X-braced frames", Earthquake Engineering and Structural Dynamics, 40(4):355-374, 2011.

[8] Roeder C.W., Lumpkin E.J., and Lehman D.E., "A Balanced Design Procedure for Special Concentrically Braced Frame Connections", Journal of Constructional Steel Research, 67(11):1760-1772, 2011.

[9] Fleischman R.B., and Hoskisson B.E., "Modular Connectors for Seismic Resistant Steel Moment Frame", Advanced Technology in Structural Engineering, 103:1-9, 2000.

[10] Fleischman R.B., Li X., Pan Y., and Sumer A., "Cast Modular Panel Zone Node for Steel Special Moment Frames. I: Analytical development", Journal of Structural Engineering, 133(10):1393-1403, 2007.

[11] Fleischman R.B., Palmer N.J., Wan G., and Li X., "Cast Modular Panel Zone Node for Steel Special Moment Frames. II: Experimental Verification and System Evaluation", Journal of Structural Engineering, 133(10):1404-1414, 2007.

[12] Sumer A., Fleischman R.B., and Hoskisson B.E., "Development of a Cast Modular Connector for Seismic-Resistant Steel Frames part I: Prototype Development", AISC Engineering Journal, 44(3):195-211, 2007.

[13] De Oliveira J., Packer J., and Christopoulos C., "Cast steel connectors for circular hollow section braces under inelastic cyclic loading", Journal of Structural Engineering, 134(3):374-383, 2008.

[14] Gray M.G., Christopoulos C., and Packer J.A., "Cast steel yielding fuse for concentrically braced frames", Proceeding of the 9th US National and 10th Canadian Conference on Earthquake Engineering, July 25-29, Ottawa, ON, Canada, 2010.

[15] Gray M.G., Christopoulos C., Packer J.A., and Lignos D.G., "Development, Validation and Modeling of the new Cast Steel Yielding Brace System", Proceedings of the 20th Analysis and Computation Specialty Conference, Chicago, JOT, USA, 2012.

[16] Gray M.G., Christopoulos C., and Packer J.A., "Cast Steel Yielding Brace System for Concentrically Braced Frames: Concept Development and Experimental Validations", Journal of Structural Engineering, 140(4):1-11, 2014.

[17] Federico G., "Use of Cast Modular Components for Concentrically Braced Steel Frames", PhD Thesis, University of Arizonza, AZ, USA, 2012.

[18] Ward K.M., Fleischman R.B., and Federico G.A., "Cast modular bracing system for steel special concentrically braced frames", Engineering Structures, 45:104-116, 2012.

[19] Federico G., Fleischman R.B., and Ward K.M., "Buckling control of cast modular ductile bracing system for seismic-resistant steel frames", Journal of Constructional Steel Research, 71:74-82, 2012.

[20] Balut N., and Gioncu V., "Suggestion for an improved 'dog-bone' solution", Proceedings of the 4th International Conference on Behavior of Steel Structures in Seismic Areas, Naples, Italy, 2003.

[21] Stevens D., and Wiebe L., "Experimental Testing of a Replaceable Brace Module for Seismically Designed Concentrically Braced Steel Frames", Journal of Structural Engineering, 145(4):1-11, 2019.

[22] Zhao J.X., Chen R.B., Wang Z., and Pan Y., "Sliding corner gusset connections for improved buckling-restrained braced steel frame seismic performance: Subassemblage tests", Engineering Structures, 172:644-662, 2018.

[23] Zhao J.X., Yu H.C., Pan Y., Chen R.B., and Guo R., "Seismic performance of sliding gusset connections in buckling-restrained braced steel frame", Journal of Building Structures, 40(02):117-127, 2019.

[24] AISC 341-16. Seismic provisions for structural steel buildings, American Institute of Steel Construction, Inc, Chicago, IL, USA, 2016.

[25] Okazaki T., Dimitrios G.L., Mitsumasa M., James M.R., and Jay L., "Damage to steel buildings observed after the 2011 Tohoku earthquake", Earthquake Engineering Research Institute, 29(1_suppl):219–243, 2013.

[26] Wakabayashi M., "Experiments on the elastic-plastic behavior of bars subjected to cyclic axial loads", Proceedings of Annual Meeting, October, Japan, 1972.

[27] Watanabe A., Hitomi Y., Saeki E., Wada A., and Fujimoto M., "Properties of brace encased in buckling-restraining concrete and steel tube", Proceeding of the 9th World Conference on Earthquake Engineering, August 2-9, Toyko, Kyoto, Japan, 1988.

[28] Tsai K.C., Lai J.W., Hwang Y.C., and Lin S.L., "Research and application of double-core buckling restrained braces in Taiwan", 13th World conference on earthquake engineering, August 1-6, Vancouver, BC, Canada, 2004.

[29] Jia M.M., Li L., Hong C., Liu K., and Sun L., "Experiment of hysteretic behavior and stability performance of buckling-restrained braced composite frame", Advanced Steel Construction, 17(2):149-157, 2021.

[30] Shi, Y., Qian, H., Kang, L., Li, Z., and Xia, L., "Cyclic behavior of superelastic SMA cable and its application in an innovative self-centering BRB", Smart Materials and Structures, 30(9): 095019, 2021.

[31] Zhang, C., Zong, S., Sui, Z., and Guo, X., "Seismic performance of steel braced frames with innovative assembled self-centering buckling restrained braces with variable post-yield stiffness", Journal of Building Engineering, 64:105667, 2023.

[32] Hu, B., Min, Y., Wang, C., Xu, Q., and Keleta, Y., "Design, analysis and application of the double-stage yield buckling restrained brace", Journal of Building Engineering, 48:103980,2022.

[33] Lu, Y., Liu, Y., Wang, Y., Liu, J., and Huang, X., "Development of a novel buckling-restrained damper with additional friction energy dissipation: Component tests and structural verification", Engineering Structures, 274:115188, 2023.

[34] Yue Y.C., Bai Y.T., Wang Y., Ma X.F., Wang Y.H., and Li X.H., "Experimental behavior and design of rectangular concrete-filled tubular buckling-restrained braces", Advanced Steel Construction, 17(4):366-375, 2021.

[35] Xie L.Q., Wu J., Shi J.H., and Zhu Y.Q., "Influence of the core-restrainer clearance on the mechanical performance of sandwich buckling-restrained braces", Advanced Steel Construction, 16(1):37-46, 2020.

[36] Yin Z.Z., Chen W., Chen S.L., and Wang X.L., "Experimental study of improved double-tube buckling restrained braces", Journal of Building Structures, 35(09):90-97, 2014. (in Chinese)

[37] Yin Z.Z., Yang B., and Zhang X.B., "Design of an eccentrically buckling-restrained braced steel frame with web-bolted replaceable links", Journal of Constructional Steel Research, 192:1-18, 2022.

[38] Yin Z.Z., Yang B., and An S.Z., "Seismic Performance Analysis of Buckling-Restrained Braced Steel Frames with Ductile Castings", KSCE Journal of Civil Engineering, 25(10):1-18, 2021.

[39] Yin Z.Z., Xu D.Y., and Yang B., "Experimental study of prefabricated buckling-restrained braces with ductile casting connectors", Journal of Building Structures, 43(1):77-85, 2022. (in Chinese)

[40] GB 50011-2010. Code for Seismic Design of Buildings, China Ministry of Construction, Beijing, China.

[41] JGJ 99–2015. Technical specification for steel structure of tall building, China Ministry of Construction, Beijing, China.

[42] Bao S.H., Structural design of high-rise building, China Architecture & Building Press, Beijing, China.

[43] Li J.M., "Experimental study on buckling restrained brace with ductile connectors", MS Thesis, Lanzhou University of Technology, Lanzhou, China, 2019. (in Chinese)

[44] Yin Z.Z., Feng D.Z., Yang B., and Pan C.C., "The Seismic Performance Analysis of Double Tube Buckling Restrained Brace with Cast Steel Connectors", Advanced Steel Construction, 18(1):436-445, 2022.

[45] Xu D.Y., "Research on Mechanical Properties of Special Centrically Braced Steel Frame with the Weakened Ductile Connectors", MS Thesis, Lanzhou University of Technology, Lanzhou, China, 2020. (in Chinese)

[46] GB/T 228.1-2010. Tensile testing of metallic materials—Part 1: Room temperature test methods, General Administration of Quality Supervision, Inspection and Quarantine, Beijing, China.

[47] GB/T 2975-2018. Steel and steel products-Location and preparation of samples and test pieces for mechanical testing, State Administration for Market Regulation, Beijing, China.

[48] JGJ/T 101-2015. Specification for seismic test of buildings, China Ministry of Construction, Beijing, China.